Nanoscale

PAPER

View Article Online
View Journal | View Issue

Cite this: *Nanoscale*, 2022, **14**, 18041

Trapping of protein cargo molecules inside DNA origami nanocages†

Merle Scherf,[a,b] Florian Scheffler,[a,b] Christopher Maffeo,[c] Ulrich Kemper,[b] Jingjing Ye,[b,d] Aleksei Aksimentiev, [c,e] Ralf Seidel [b,d] and Uta Reibetanz *[a]

The development of the DNA origami technique has directly inspired the idea of using three-dimensional DNA cages for the encapsulation and targeted delivery of drug or cargo molecules. The cages would be filled with molecules that would be released at a site of interest upon cage opening triggered by an external stimulus. Though different cage variants have been developed, efficient loading of DNA cages with freely-diffusing cargo molecules that are not attached to the DNA nanostructure and their efficient retention within the cages has not been presented. Here we address these challenges using DNA origami nanotubes formed by a double-layer of DNA helices that can be sealed with tight DNA lids at their ends. In a first step we attach DNA-conjugated cargo proteins to complementary target strands inside the DNA tubes. After tube sealing, the cargo molecules are released inside the cavity using toehold-mediated strand displacement by externally added invader strands. We show that DNA invaders are rapidly entering the cages through their DNA walls. Retention of ~70 kDa protein cargo molecules inside the cages was, however, poor. Guided by coarse-grained simulations of the DNA cage dynamics, a tighter sealing of the DNA tubes was developed which greatly reduced the undesired escape of cargo proteins. These improved DNA nanocages allow for efficient encapsulation of medium-sized cargo molecules while remaining accessible to small molecules that can be used to trigger reactions, including a controlled release of the cargo *via* nanocage opening.

Received 28th September 2022,
Accepted 18th November 2022

DOI: 10.1039/d2nr05356j

rsc.li/nanoscale

Introduction

Rapid developments in the field of synthetic bio-nanotechnology established ample opportunities to fabricate nanometer-sized tools for the controlled sensing, probing and manipulation of molecules and nanoparticles. Particularly, nucleic acid nanotechnology attracted considerable interest due to the ease at which diversely shaped nanostructures can be encoded by nucleic acid sequences.[1–3] The development of the DNA origami technique enabled the production of MDa-sized DNA nanostructures at high yield and purity in simple one-pot reactions.[4,5] Many applications emerged ranging from the construction of three-dimensional nanostructures,[6] the establishment of molecular machines, such as nanorobots and walkers,[7–9] drug delivery,[10,11] artificial cell membrane channels,[12,13] functional bioanalytical devices, such as enzymatic reactors,[14] to nanophotonic and nanoelectronics devices.[15–18]

In particular, the development of DNA origami nanocages with cavities to encapsulate molecules or nanoparticles of interest opened up the opportunity for targeted and specific drug delivery as they can be equipped with multiple functions. Such functions include the addition of cargo molecules, the assembly of switchable elements for triggered opening, and the integration of stabilizing factors to protect the nanocages from early degradation by serum proteins or endolysosomal enzymes.[19–23] Hence, the basis is available for generating a device for time- and amount-controlled application of therapeutics at defined intracellular target sites. It also allows to overcome specific limitations in drug delivery, such as by the intercalation of weak basic agents as doxorubicin into the DNA nanostructure.[24]

As a first step, DNA-based drug delivery systems were established with internally bound cargos to be transported to cells, as already realized with antibody fragments,[7,25] horseradish

[a]*Institute for Medical Physics and Biophysics, Medical Faculty, University of Leipzig, Härtelstraße 16-18, 04107 Leipzig, Germany.*
E-mail: uta.reibetanz@medizin.uni-leipzig.de
[b]*Peter Debye Institute for Soft Matter Physics, Faculty of Physics and Earth Science, University of Leipzig, Linnéstraße 5, 04103 Leipzig, Germany*
[c]*Department of Physics, University of Illinois at Urbana–Champaign, 1110 W Green St, Urbana, IL 61801, USA*
[d]*Cluster for Advancing Electronic Devices Dresden, University of Dresden, Helmholtzstraße 18, 01069 Dresden, Germany*
[e]*Department of Physics and Beckman Institute for Advanced Science and Technology, University of Illinois at Urbana–Champaign, 405 N Mathews Ave, Urbana, IL 61801, USA*

† Electronic supplementary information (ESI) available. See DOI: https://doi.org/10.1039/d2nr05356j

peroxidase,[8] doxo- and daunorubicin molecules[24,26] and serum albumin.[23] However, in contrast to the simplest idea of freely diffusing, untethered molecules inside a closed container, cargo molecules were so far firmly attached to the origami nanostructures. A therapeutic effect in such a case could then only be initialized by two different mechanism: on one hand, controlled opening of the structures upon cell attachment[7] allows the internally bound agents to come into physical contact with the surface of cells; on the other hand, therapeutically active molecules or nanoparticles can be internalized by cells *via* (receptor mediated) endocytosis of the filled nanostructures[27,28] followed by their complete disassembly within endolysosomes.

Though, DNA origami-bound enzymatic cargo can exhibit an increased activity,[29] the free diffusion of the large superstructure may strongly be hindered inside of cells. Targeted transport of active or therapeutic agents into selected cell compartments such as the cytoplasm or close to the nucleus requires however the immediate accessibility of the agent once released from its transport device. Consistently, the combination of freely diffusing cargo within a nanocarrier combined with controlled nanocarrier opening by switch elements[7,30] provides the opportunity to develop an even more specific drug delivery system by using the DNA origami technology: a locked box containing unbound active agents which can be set free after triggered opening of the lids.

However, to realize such a triggered release, the origami nanostructures have to be first filled with the freely diffusing molecules that are not bound to the nanostructures. Accomplishing this requires dense, impenetrable DNA walls that inhibit an undesired escape of the cargo despite their intrinsic flexibility and dynamics, which is potentionally difficult to achieve.[31] In this work, we address the so-far unresolved challenges for the development of origami nanocages that can retain freely diffusing molecules as a prerequisite for the controlled release by external triggers. We designed and prepared nanocages consisting of DNA origami nanotubes with square cross section that can be closed by docking DNA origami lids onto each tube end. To allow efficient loading of a protein cargo into the nanotubes at experimentally accessible concentrations, the proteins were first conjugated with single-stranded DNA (ssDNA) before being anchored in the open tubes to complementary ssDNA target strands.[23,32] Subsequent addition of the lids allowed their encapsulation. In order to release the cargo into the nanocage cavities, we applied toehold-mediated strand displacement.[33,34] We could demonstrate that externally added ssDNA invader strands rapidly enter the origami nanocages and displace the target-bound cargo. Surprisingly, we observed that the cages did not sufficiently retain medium-sized protein molecules such as streptavidin and BSA. Coarse-grained simulations of the DNA cage dynamics revealed that the proteins escaped through gaps at the interface of the tube with the lids. Using improved lid versions with minimized gaps provided great reduction of protein escape. We expect that our improved DNA origami nanocages that can retain untethered protein cargo molecules will expand the DNA-based toolbox for drug delivery. Furthermore, our results provide an interesting insight into the diffusive passage of biomolecules through DNA nanostructures.

Results and discussion

Strategy for loading DNA nanocages with cargo molecules

We based our DNA origami nanocages on DNA origami nanotubes of 40 nm length and quadratic cross section with ~25 nm edge length that have been previously used as molds for gold nanoparticle fabrication.[35] The tube wall was formed by a double layer of 10 DNA helices in an array such that the quadratic cavity cross section had an edge length of ~15 nm (Fig. 1a-left and ESI Fig. S1†). The nanotubes could be sealed on each side using DNA origami lids that were formed by a 10 × 10 array of parallel DNA helices on a square lattice forming a tightly packed block of DNA (Fig. 1a-middle).[16,23] The pattern of recessed and protruding helix ends at the outer two layers of the lid matched the pattern of the DNA ends of the tube walls such to support a seamless docking of the lids onto the tube ends. Both, lids and nanotubes exhibited a structural polarity,[23] such that only the right lid end could seamlessly dock onto the left tube end and, correspondingly, the left lid end onto the right tube end (Fig. 1a-right, and ESI Fig. S1b and c†). To support specific docking of the lids to the corresponding tube end, 40 of the 64 DNA ends that were involved in the docking were chosen to have attractive ends. They were

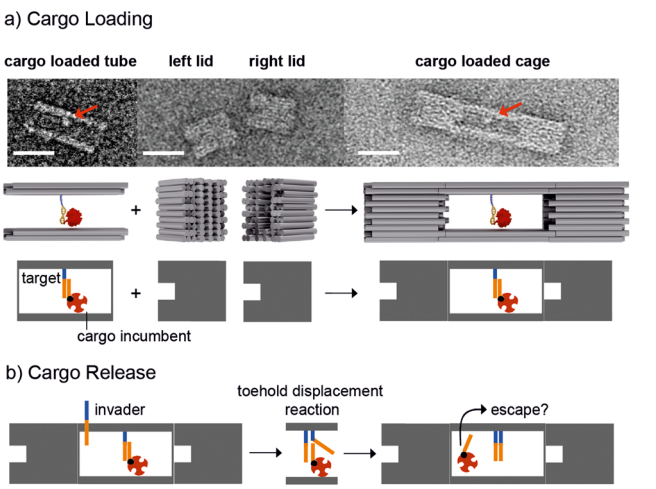

Fig. 1 Scheme of the loading of DNA origami nanocages with freely diffusing cargo molecules. (a) Protein cargo molecules conjugated to an ssDNA strand are beforehand annealed to a complementary target strand inside DNA origami nanotubes. By adding origami lids, a stable cargo-loaded origami cage is created. The upper row shows representative TEM images of the cargo loaded tube, the lids and the cargo loaded cage with a scale bar of 30 nm. The red arrows point at a streptavidin-cargo molecule. (b) Adding an invader strand that can bind to the toehold region on the target (blue) allows the release of the cargo from the capture strand by strand displacement. Released cargos may either remain within the cage or inadvertently escape from it.

formed by 2 nt overhangs of the staple ends on one side that could hybridize to the scaffold on the other side where the staples were correspondingly recessed by 2 nt (ESI Fig. S1–S3†). The remaining 24 DNA ends were made repulsive by adding 6 nt overhangs with the same sequence to the staple ends. The specific pattern of attractive and repulsive helix ends as well as the usage of either 5′ overhangs (right interface) or 3′ overhangs (left interface) allowed to form highly specific interfaces (ESI Fig. S1†).[35] Additionally, for all DNA helices of the lid that were not involved in the tube sealing, repulsive ends were used in order to prevent unspecific binding. After incubating the tubes and both lids overnight using a 1 : 1.1 : 1.1 stoichiometry, trimeric nanocages were formed in a high yield (ESI Fig. S4†).

To allow loading of ssDNA-conjugated cargo molecules, the nanotubes contained a central ssDNA target strand extending from helix 24 (ESI Fig. S1 and S3†). This allowed the attachment of cargo-bound DNA strands (furthermore called incumbents) by hybridization leaving a 10 nt region of unpaired bases on the target serving as toehold for a subsequent cargo release. After nanotube loading, lids were added and a closed trimeric structure was formed that encapsulated the cargo molecule inside a DNA cage (Fig. 1a-right).

To provide controlled detachment of cargo molecules from the cavity walls, we aimed to use toehold-mediated strand displacement by externally adding DNA invader strands that are complementary to the target including the toehold region (Fig. 1b). The efficiency of invader entry into the highly negatively charged DNA cages remained, however, to be determined. After detachment, the cargo molecules should remain freely diffusing within the cage (Fig. 1b-right) until a controlled lid opening (*e.g.* within a desired cell compartment). Eventually, small cargo molecules may also unintentionally escape through the cage walls, particularly at defect sites.

Strand displacement inside DNA nanotubes and nanocages using external invaders

To realize the envisioned loading scheme of DNA nanocages with unbound cargo molecules, we first tested whether the origami wall structure would be permeable for the 27 nt ssDNA invader strands that would promote the strand displacement inside the cages. We followed this process *via* fluorescence detection using Cy3-labeled invader and Cy5-labeled incumbent strands (Fig. 2a).

We added the invaders to either incumbent-containing nanotubes or nanocages and analyzed the reaction products after different incubation times using agarose gel electrophoresis. Analyzing the Cy3 fluorescence of the invaders revealed a rapid invader accumulation in the DNA tubes and cages being almost complete within the first 30 min (Fig. 2b, white box marking green fluorescence signals of origami nanostructures). Analyzing the Cy5 fluorescence of the nanotube- and nanocage-bound incumbents revealed in parallel an almost complete incumbent detachment within the first 30 min and its migration into the supernatant (Fig. 2b, white box marking red fluorescence signals of origami nanostructures). During these measurements, the trimeric origami nanocages remained intact (ESI Fig. S5a†). Thus, our results unambiguously demonstrated an efficient strand displacement reaction not only inside the nanotubes, but also in the nanocages. Interestingly, within our time resolution, we obtained the same strand displacement kinetics for the open nanotubes as well as the closed nanocages. Thus, despite the high negative charge of the phosphate groups of nucleic acid, the DNA invader strands could rapidly pass the DNA double layer of the tube walls at the given ionic conditions. Likewise, the released DNA incumbents could rapidly diffuse out of the cage structures.

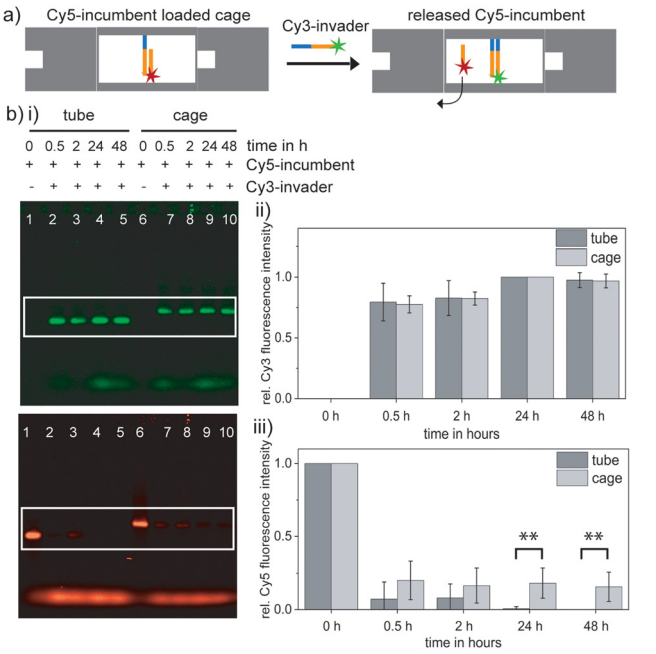

Fig. 2 Strand displacement reaction inside DNA origami nanotubes and nanocages with externally added DNA invader strands. (a) Scheme of the reaction employing a Cy5-labeled incumbent and a Cy3-labeled invader. (b) Monitoring the Cy3-invader binding (i, upper part) and Cy5-incumbent release (i, lower part) over time inside nanotubes and nanocages using agarose gel electrophoreses and detecting the Cy3 and Cy5 fluorescence, respectively. Quantitative analysis of the band intensities of the nanotubes and nanocages inside the white boxes are shown for the invader binding (ii) and for the incumbent release (iii). The band intensities at 24 h (ii) and 0 h (iii) were used for normalization for Cy3 and Cy5 fluorescence. Data points represent mean values with corresponding standard deviations. Significances were obtained using a one-tailed Student's *t*-test with $*p \leq 0.05$, $**p \leq 0.01$, $***p \leq 0.001$.

Release of streptavidin-conjugated incumbents inside origami nanotubes and nanocages

After successfully establishing strand displacement inside the origami nanotubes and nanocages by externally added DNA invaders, we tested the release of cargo-bound incumbents within the nanotube cavity. We first used streptavidin as a cargo. The streptavidin tetramer has a molecular weight of 53 kDa, a size of about 5.4 × 5.1 × 4.2 nm and a slight negative charge under our experimental conditions (pI of 6–7) (ESI

Fig. S6a†). To set-up and monitor the release reaction, we bound Cy5-labeled streptavidin to 5′-biotinylated incumbent strands which were subsequently hybridized to the target strands inside the DNA nanotubes. The loading step was followed by lid addition to encapsulate the protein inside DNA nanocages (Fig. 3a). Successful and stable cage formation during the experiment was probed by agarose gel electrophoresis and ethidium bromide staining (ESI Fig. S5b†).

To trigger the protein release from the target strand, we added DNA invader strands to streptavidin-loaded nanotubes and nanocages (Fig. 3b). Initially, a bright fluorescent signal was observed at the nanotube and nanocage positions indicating successful loading of streptavidin. Surprisingly, upon invader addition, the signal became greatly reduced for both nanostructures already within the first 30 min after invader addition. Shorter times were not accessible, since we used polyethylene glycol (PEG) precipitation as a reaction stop (see Experimental). Omitting PEG purification allowed however to directly reveal the protein release (Fig. S5b†).

This indicated that the streptavidin-incumbent complex could not only escape from the open nanotubes but also from the closed nanocages with similar kinetics. The nanocages retained only marginally more streptavidin than the nanotubes (3% *vs.* 1% after 48 h). Considering an average inter-helical distance of about 0.6 nm for the square lattice structure,[36] a much bigger cargo inside the nanocage is not expected to escape rapidly. To exclude that the rapid streptavidin escape from the nanocages was due to externally bound streptavidin occurring in the preparation process, we applied TEM imaging. After loading, single streptavidin complexes could be readily observed in the centres of origami nanotubes and nanocages (Fig. 3c, and ESI Fig. S7a†). Externally bound protein was not observed. When adding invader, the TEM investigations illustrated that the loading efficiencies for cargo-incumbent on nanotubes and nanocages became reduced already within the first 2 h (Fig. 3b and ESI Fig. S7a†). This agrees with the electrophoresis results and provides solid evidence for escape of the protein from the nanocage cavities.

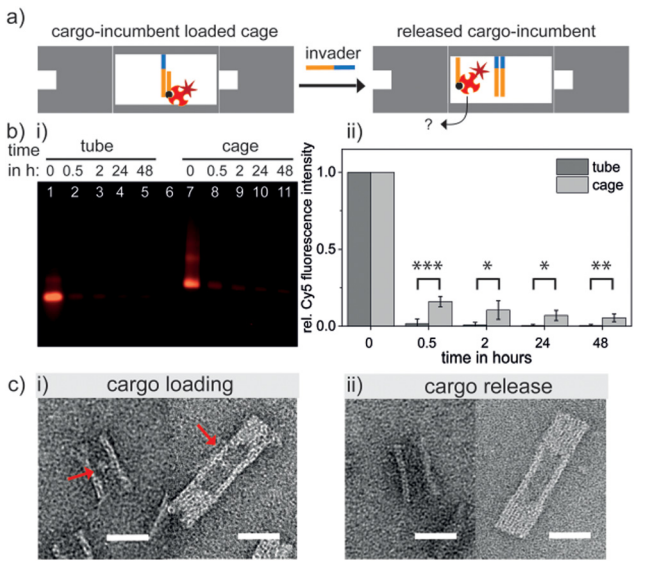

Fig. 3 Strand displacement and escape of streptavidin-conjugated incumbents bound inside DNA origami nanotubes and nanocages with externally added invader. (a) Scheme of the reaction employing a Cy5-labeled streptavidin bound to biotinylated incumbent strands and unlabeled DNA invaders. (b) Monitoring streptavidin-incumbent escape over time from the cavities of origami nanotubes and nanocages using agarose gel electrophoresis after removing free invaders and released streptavidin incumbents by PEG purification. Shown are the gel image detecting the Cy5 fluorescence (i) together with a quantitative analysis of the origami band intensities (ii). The band intensities at 0 h were used for normalization. (c) Representative TEM images of origami nanotubes and nanocages loaded with streptavidin incumbents before (i, see red arrows) and 48 h after incumbent release (ii). Scale bars are 30 nm. Data points represent mean values with corresponding standard deviations. Significances were obtained using a one-tailed Student's *t*-test with $*p \leq 0.05$, $**p \leq 0.01$, $***p \leq 0.001$.

Migration of streptavidin-conjugated invaders into origami nanotubes and nanocages

The surprising finding that a ~5 nm-sized streptavidin molecule could escape from the nanocage cavities led us to the question of whether externally added invader-bound streptavidin molecules could likewise enter nanotubes and nanocages. For monitoring this process, we used Cy5-labeled streptavidin that was attached to the invader by a biotin modification (Fig. 4a) and analyzed its binding in the nanotube cavity by gel electrophoresis. While streptavidin–invader binding inside the open nanotubes was almost complete within the first 30 min, it extended over several hours and was much less efficient inside the fully assembled nanocages (Fig. 4b, and ESI Fig. S5c†). After 48 h only 30% of the streptavidin migrated into the nanocages compared to the open nanotubes. Monitoring streptavidin binding inside the nanotube and nanocage cavities using TEM imaging qualitatively supported these results (Fig. 4c and ESI Fig. S7b†). Streptavidin binding was fast for open nanotubes (<2 h), but significantly slower and less efficient inside the nanocages.

Overall, we can conclude from these results that nanotube closure by the lids significantly slows down the migration of streptavidin into the cages. In turn it should also slow down the migration out of the sealed nanocages. The fact that we did observe a faster kinetics for streptavidin escape from the nanocages compared to invasion can be explained by locally higher concentration inside the cages. Additionally, we can conclude that the cargo size matters for the migration through the cage walls, since streptavidin-bound invaders only slowly enter the nanocages (Fig. 4b) in contrast to pure DNA invaders (Fig. 2b).

Release of BSA-conjugated incumbents inside origami nanotubes and nanocages

To test whether the rapid escape of proteins from origami nanocages is protein specific, we carried out similar experiments for bovine serum albumin (BSA), a mostly monomeric protein with a molecular weight of 66 kDa and a slightly more negative charge (pI = 4.7). Compared to streptavidin it has a

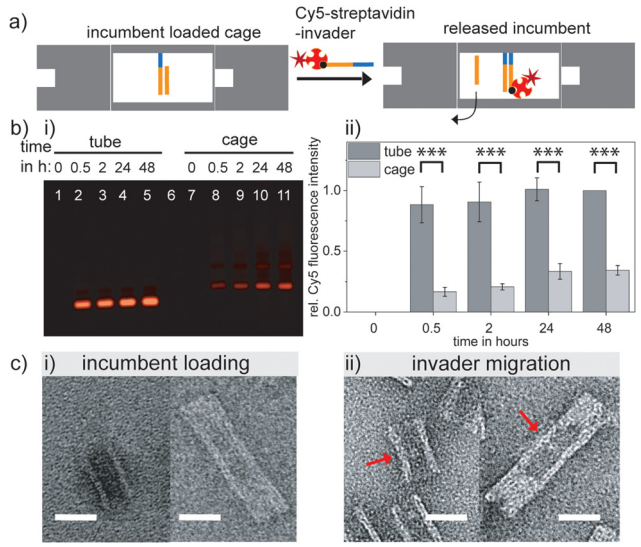

Fig. 4 Strand displacement reaction inside origami nanotubes and nanocages with externally added streptavidin-conjugated invader strands. (a) Scheme of the reaction employing unlabeled incumbent strands and Cy5-labeled streptavidin attached to biotinylated invader strands. (b) Monitoring streptavidin–invader binding over time inside nanotubes and nanocages using agarose gel electrophoreses after removing free streptavidin invaders by PEG purification. Shown is the gel image detecting Cy5 fluorescence (i) together with a quantitative analysis of the band intensities (ii). The band intensity of the tube at 48 h was used for normalization. (c) Representative TEM images of unlabeled incumbent loaded nanotubes and nanocages showing empty cavities (i) and streptavidin invader-containing nanotubes and nanocages after 48 h marked with red arrows (ii) are shown below. Scale bars are 30 nm. Data points represent mean values with corresponding standard deviations. Significances were obtained using a one-tailed Student's *t*-test with $*p \leq 0.05$, $**p \leq 0.01$, $***p \leq 0.001$.

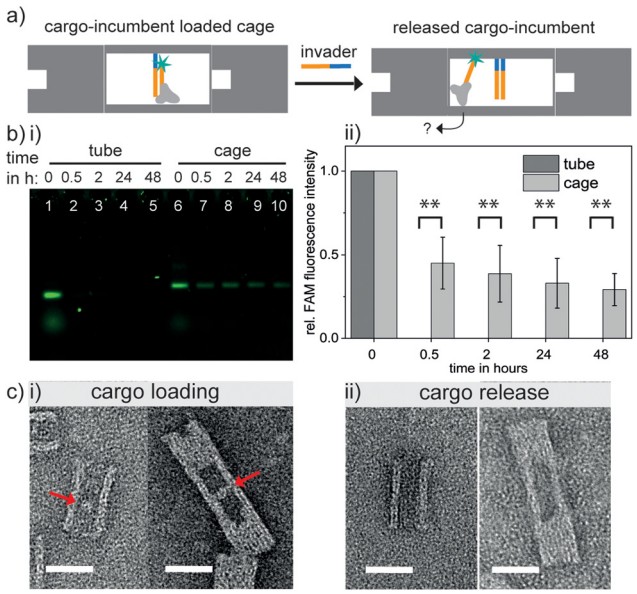

Fig. 5 Strand displacement and escape of BSA-conjugated incumbents bound inside origami nanotubes and nanocages by externally added invader. (a) Scheme of the reaction employing a FAM-labeled incumbent that was covalently attached to BSA and unlabeled DNA invaders. (b) Monitoring BSA-incumbent escape over time from the cavities of nanotubes and nanocages using agarose gel electrophoreses after removing free invaders and released BSA-incumbents by PEG purification. Shown is the gel image detecting FAM fluorescence (i) together with a quantitative analysis of the band intensities (ii). The band intensities at 0 h for nanocages and nanotubes were used for normalization. (c) Representative TEM images of BSA incumbent-containing nanotubes and nanocages that are marked with red arrows (i) and released BSA-incumbent after 48 h (ii) are shown below. Scale bars are 30 nm. Data points represent mean values with corresponding standard deviations. Significances were obtained using a one-tailed Student's *t*-test with $*p \leq 0.05$, $**p \leq 0.01$, $***p \leq 0.001$.

similar weight but appears with its dimensions of 8.3 × 6.0 × 3.0 nm (ESI Fig. S6b†) slightly more elongated but of similar diameter. For the loading of BSA into the tube cavities and monitoring its release, the protein was conjugated with azido benzoate-modified and FAM-labeled incumbent strands (Fig. 5a). The successful conjugation and removal of FAM-labeled incumbents without BSA was analyzed *via* gel electrophoresis (ESI Fig. S8†).

When adding invader strands to BSA-loaded nanotubes, a complete detachment and escape of BSA was observed within the first 30 min. For the origami nanocages only more than 50% of the BSA escaped in the first 30 min followed by a further minor escape in the subsequent hours (Fig. 5b) such that ~30% of the initially bound BSA molecules remained after 48 h. This result was also supported by TEM imaging (Fig. 5c), demonstrating a rapid and complete escape of BSA-incumbents from the nanotubes but only a limited escape from the nanocages. The increased retention of BSA compared to streptavidin suggests that cargo size and/or charge can affect the migration through the cage walls. Stability of the nanocages during the experiment were probed by agarose gel electrophoresis and ethidium bromide staining (ESI Fig. S5d†).

Coarse-grained simulations of cargo release from origami nanocages

The escape of a relatively large protein cargo from the DNA cages was quite surprising, given the narrow spacings between the DNA helices in the cage structures. Generally, escape could occur through the cages walls where transient cavities could form due to lateral fluctuations of the DNA helices in between crossovers, at defect sites or at the interface between DNA tubes and the lids. For the latter, special attention should be drawn onto the positions of repulsive DNA ends (see ESI Fig. S9†), at which the sealing of the cages by the lids may be less tight.

To investigate the pathways of cargo escape from origami nanocages on the microscopic level, we carried out mrDNA coarse-grained simulations.[37] Particularly, we studied the escape of spherical cargo with radii ranging from 0.4 nm to 2 nm. Small cargo (0.4–0.6 nm radius similar to invader and incumbent strands) was predominantly leaving the cages through transient apertures in the plane cage walls (Fig. 6a). Larger cargo (>0.8 nm radius) escaped, however, exclusively at the interfaces between tube ends and lids. Within the simu-

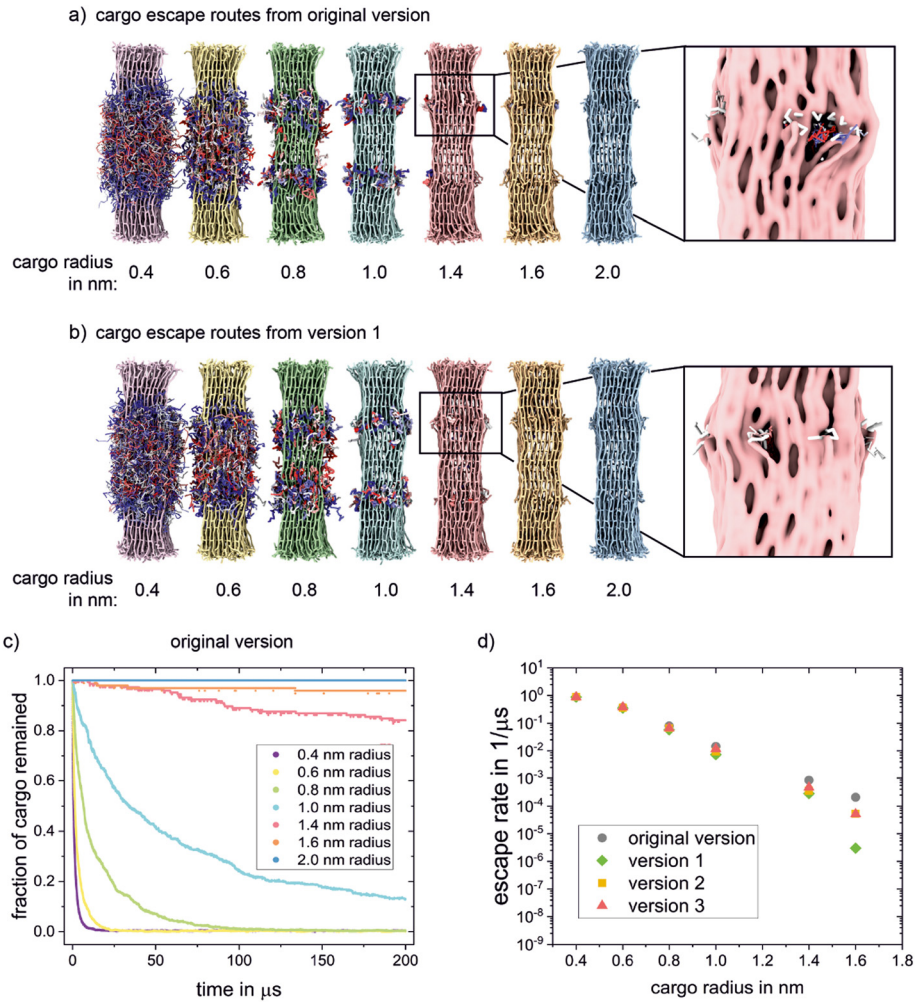

Fig. 6 Simulation of the escape of differently sized cargo from a DNA origami nanocage with constant diffusion coefficients. (a) Monitoring the escape routes of the cargo (radii between 0.4 nm–2 nm) out of the original origami cages with a close-up picture for the escaping of cargo with 1.4 nm radius out of the origami nanocage shown with surface mesh. (b) Monitoring the escape routes of the cargo out of the origami cage version 1 with a close-up picture for escaping of a cargo with 1.4 nm radius. (c) Cargo fraction remaining inside the cages of the original version as function of time for the different cargo radii. (d) Mean escape rate of the cargo as function of the cargo radius. Shown are results for the original nanocage design as well as for the tighter cage versions 1–3. Note the logarithmic scale of the escape rate values.

lation time of 200 μs, we obtained cargo escapes for radii of up to 1.6 nm. Increasing the cargo size was accompanied by slower release kinetics (Fig. 6c). The mean escape rate decreased approximately exponentially with the cargo radius despite the different escape routes (Fig. 6d), such that escape of even larger, *e.g.* protein-sized, cargo may be possible on longer time scales. Similar to the behaviour observed for passive transport of large cargo through a nuclear pore complex,[38] the rate of the protein cargo escape is likely determined by the probability of spontaneously forming a void in the DNA origami enclosure large enough to accommodate the cargo.

When inspecting the escape positions more closely, we noticed that they corresponded to regions with multiple consecutive repulsive ends as predicted before (ESI Fig. S9†). The repulsive helix ends at these positions underwent significant lateral fluctuations (close-up Fig. 6a), providing the formation of transient gaps between lid and tube end. Such gaps were not present at attractive helix end positions.

Design and characterization of tighter lid–tube interfaces

To reduce transient gap formation and cargo escape at the lid–tube interfaces, we thought to eliminate consecutive repulsive ends to achieve a tighter sealing of the nanotubes by the lids. Designing an interface version containing no repulsive but only attractive DNA ends resulted however in highly unspecific binding supporting even lid–lid and mold–mold interactions such that highly heterogeneous assemblies were formed (ESI Fig. S10†).

As our next design, we isolated the repulsive ends in the interface designs and avoided any consecutive arrangements of repulsive ends. We designed three versions containing

either 16 (version 1), 18 (version 2) or 22 (version 3) repulsive ends (see ESI Fig. S11a, S12 and S13†). Inspecting the resulting origami nanotubes and lids *via* gel electrophoresis (ESI Fig. S11b†) as well as non-specific aggregation formation of some of the monomers by TEM imaging (ESI Fig. S11c†) but a highly specific and efficient formation of trimeric origami nanocages for all interface versions (ESI Fig. S11d†), demonstrate a successful redesigning of the nanocage.

Next, we used mrDNA simulations to test cargo escape from the new nanocage versions. We found the escape routes of the molecules from version 1 cages to be similar to those of the original version: small cargos up to 0.6 nm in radius permeate through the entire cage structure whereas larger cargos (>0.8 nm radius) escape through the tube lid interfaces. However, a smaller amount of cargo molecules was observed to escape from the new cage designs (Fig. 6b). For cargos up to 1.4 nm in radius, the escape kinetics and the mean escape rates appeared only slightly reduced compared to the original version (Fig. 6c and ESI Fig. S14†), with no major differences between versions 1, 2 and 3. But for version 1 design we observed several orders of magnitude reduction of the cargo escape rate at 1.6 nm radius cargos. This indicates that, in the improved cage designs, the size of transient gaps at the lid–cage interface is reduced, causing a rather sharp size cut-off for permeation of larger cargos.

Next, we tested experimentally whether the new nanocage versions better prevented the escape of streptavidin incumbents compared to the original design (Fig. 7a). Analyzing the escape of streptavidin from the origami nanocages using gel electrophoresis revealed for the new interface versions a sudden reduction of the bound streptavidin to 40–50% within the first 30 min. This was followed by just a minor release in the next hours to about 30% such that much more streptavidin was retained compared to the original interface design (Fig. 7b and c). We ensured that the retention of streptavidin in the new nanocage versions was not due to an insufficient amount of added invader nor to a locally high streptavidin concentration on the outside of the nanocages (see ESI Fig. S15†). Together, this confirms a tighter sealing of the nanocages in the new designs. In agreement with the simulations, no major differences in the release kinetics were found between the different new versions.

The initial sudden release of a significant fraction of the protein after 0.5 h indicated a structural heterogeneity of the cage population similar as for BSA. Analyzing the nanocage assembly with TEM imaging did, however, not reveal any major visible assembly defects (ESI Fig. S11†). We therefore attributed the observed heterogeneity to small scale assembly defects of the individual origami monomers, such as missing staples or a local misfolding. Similar findings were observed in previous studies of gold growth inside origami tubes resulting in recurring leakage of the gold growth.[39]

TEM imaging qualitatively confirmed a significant amount of streptavidin inside version 1 nanocages even 48 h after its detachment from the cage walls in contrast to the original version (ESI Fig. S7c†). To provide evidence that the cargo

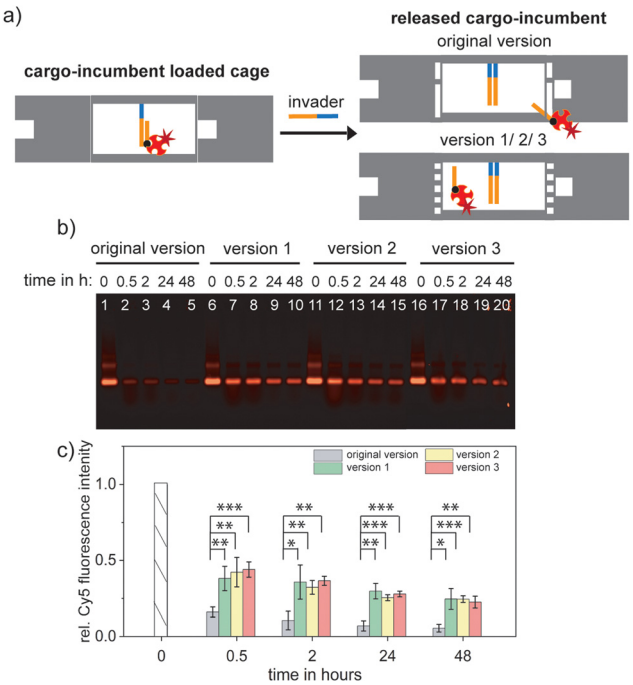

Fig. 7 Strand displacement and escape of streptavidin-conjugated incumbents from origami nanocages with tighter lids. (a) Scheme of the reaction employing as cargo Cy5-labeled streptavidin bound to a biotinylated incumbent. (b) Monitoring streptavidin-incumbent escape from origami nanocages by agarose gel electrophoreses for the original and the improved versions with tighter lids (version 1, version 2, version 3) after removing free invaders and released streptavidin-incumbents by PEG purification. (c) Quantitative analysis of the origami band intensities from b. The band intensity at 0 h was used for normalization. Data points represent mean values with corresponding standard deviations. Significances were obtained using a one-tailed Student's *t*-test with $*p \leq 0.05$, $**p \leq 0.01$, $***p \leq 0.001$.

molecules were untethered inside the nanocages cavity, we analyzed the position of the enclosed proteins inside the cavity. After loading the nanocages with streptavidin incumbents, the proteins were exclusively localized in center of the structure. After detachment from the target strand, the proteins became distributed along the entire cavity over time (ESI Fig. S16†), indicating that they were highly mobile. Overall, these experiments show that a significant fraction of streptavidin can be retained when reducing the gaps at the interfaces.

Conclusions

In this study, we demonstrate the successful loading of DNA nanocages with freely diffusing, *i.e.* unbound, cargo molecules. Our approach required DNA-conjugated cargo molecules, such as streptavidin and BSA, that were bound to complementary target strands inside origami nanotubes. Addition of origami nanolids allowed the formation of nanocages and thus the encapsulation of the bound cargo. Subsequently, the cargo molecules were detached from the nanotube walls using strand displacement through externally added invader strands.

In the final nanocage designs a significant fraction of cages were successfully retaining the unbound cargo molecules.

A surprising finding of our study was that the medium-sized DNA invader and incumbent strands could rapidly migrate through the nanocage walls that consisted of a double-layer of DNA helices. This was supported by coarse-grained molecular dynamics simulations that showed that cargo with radii up to 1.6 nm can escape through the nanocage walls due to bending fluctuations of the DNA helices. It also agrees with previous studies, where DNA as well as protein-bound invaders were shown to migrate into cavities of DNA origami nanostructures based on hexagonal lattices.[31] A further surprising result was that even ~5 nm-sized protein cargo could exit or enter the nanocages. Guided by the coarse-grained simulations we could show that mainly dynamic gaps at repulsive ends at the tube–lid interfaces were responsible for this escape. By reducing the number of repulsive strands at the interface, the nanocages became better sealed providing a significantly prolonged encapsulation of protein cargo molecules. Overall, a further interface engineering and an elimination of assembly defects of the origami nanostructures may further improve the encapsulation efficiency of molecules of interest.

Due to the high biocompatibility, easy manufacturing and possibilities to integrate switchable elements, DNA nanocages are of high interest for the development of controllable small-molecule nanocarriers. In new therapeutical approaches such as vaccination or immunotherapeutic cancer treatment[40–43] they could allow a protected transport and targeted release of therapeutic agents into cell cytoplasm. The established encapsulation of free cargo molecules inside tight DNA nanocages presents an important step for the triggered release of active molecules at sites of interest. We anticipate that our approach will be readily applicable to a large variety of different medium-sized molecules.

Experimental

The single-stranded p8064 scaffold DNA was purchased from Tilibit Nanosystems (Garching, Germany) and reverse-phase cartridge purified DNA oligonucleotides, unless otherwise mentioned, from Merck (Darmstadt, Germany) or Eurofins MWG Operon (Ebersberg, Germany). All inorganic salts were purchased from Merck and were of reagent or analytical grade. The folding buffer corresponds to 1× FB from Tilibit, containing 5 mM Tris-HCl (pH 8.0), 1 mM ethylenediaminetetraacetic acid (EDTA) and 5 mM NaCl with additional 11 mM $MgCl_2$. The loading buffer includes the folding buffer with additional 350 mM NaCl.

DNA origami assembly, purification and analysis

The designs of the origami nanotubes and lids (see ESI Fig. S2, S3, S12 and S13†) were adapted from previous work[16] using CaDNAno.[44] The DNA origami nanostructures were assembled in a one-pot reaction containing 10 nM scaffold p8064 and 100 nM staple strands in folding buffer. After initial heating to 80 °C für 5 min the solution was cooled to 25 °C over 15 h using a non-linear heat ramp. The slowest decrease was applied between 55 °C and 45 °C. Folded origami nanostructures were purified from excess oligonucleotides by precipitation with 15% polyethylene glycol (PEG, Sigma Aldrich, Germany) with subsequent pelleting using centrifugation.[45] The quality of the folded structures was inspected by gel electrophoresis using approximately 50 fmol of the origami nanostructure, mixed with 15% Ficoll® 400 (Carl Roth, Karlsruhe, Germany) and Orange G (Sigma Aldrich) in 0.8% agarose gel (Biozym Scientific GmbH, Oldendorf, Germany) and 0.5× TBE (Sigma Aldrich) and 11 mM $MgCl_2$ at 3.5 V cm^{-1}. The DNA was subsequently stained with ethidium bromide (AppliChem, Darmstadt, Germany) and imaged using a ChemiDoc MP imaging system (Bio-rad, Germany).

Conjugation of DNA incumbent with protein cargo

Covalent BSA-incumbent complexes were prepared in two steps using a click chemistry. 2.27 pmol BSA (Sigma Aldrich) were incubated with 5.69 pmol dibenzylcyclooctyne (DBCO)-maleimide (Jena Bioscience, Germany) over night at 4 °C in 20 μL total volume with 100 mM sodium phosphate buffer (pH 7.0) supplemented with 150 mM sodium chloride. The conjugated BSA sample was 3-times purified from unbound maleimide molecules using MiniQickSpin DNA columns (Roche Life Science, Germany). The sample was then incubated for 60 h at 37 °C with 5.68 pmol incumbent strands labeled on the 3′-ends with FAM and on the 5′-ends with azidobenzoat (biomers.net GmbH, Germany). The latter forms a triazole with the DBCO-group on the protein by cycloaddition. The DNA functionalized BSA was purified using Amicon 30 kDa Cut-Off filters (Sigma-Aldrich). The purification step was repeated three times until all unbound ssDNA strands were removed (see ESI Fig. S8†).

Streptavidin-incumbent complexes were prepared by incubating 0.4 pmol Cy5-labeled streptavidin (Invitrogen, Germany) with 0.4 pmol 5′-biotinylated incumbent strands (Sigma-Aldrich) in 20 μL total volume with PBS buffer for 1 h at room temperature.

TEM imaging

For TEM imaging, the origami samples were diluted to 2.5–3.5 nM, 5 μl of the sample were placed for 5 min on a glow-discharged carbon-coated TEM copper grid (Plano GmbH, Wetzlar, Germany) to allow the adsorption of the structures on the grid. After removing the fluid with filter paper, 5 μl of a filtered 2% solution of uranyl formate (Polyscience Inc., Warrington, USA) in 25 mM NaOH was added and immediately removed before another 5 μl of the solution was added and incubated for 10 s. The fluid was removed and the grids were air dried. TEM images were taken on a JEOL JEM-2100 Plus (Jeol, Japan) transmission electron microscope at 200 kV.

Nanocage assembly and cargo loading

For cargo loading, (conjugated) incumbent strands were annealed to the target inside the DNA origami nanotube using

a 2 : 1 excess. The annealing was realized in loading buffer, by initially heating to either 40 °C (for the unfunctionalized or fluorescence labeled incumbents) or 37 °C (for the protein-conjugated incumbents) and subsequently cooling to 25 °C over 5 h or 10 h, respectively. Nanocages were assembled by incubating left lids, cargo-loaded nanotubes and right lids at a 1.1 : 1 : 1.1 stoichiometric ratio overnight in the buffer used for incumbent loading. The DNA nanostructures were subsequently purified from excess incumbents using PEG precipitation.

Cargo detachment by strand displacement

The unfunctionalized or streptavidin-conjugated invaders were added to 12.5 nM of the loaded origami tube or cage structures in 10 µl loading buffer at a 2-fold excess to reach a reaction concentration of 10 nM for the DNA nanostructure. After specified times (typically 0.5 h/2 h/24 h/48 h) the sample were withdrawn for gel electrophoresis. Samples containing protein-conjugates incumbents or invaders were before purified by PEG precipitation to stop the reaction and to remove unbound proteins as they migrated similarly as the origami nanostructures during gel electrophoresis and interfere with the corresponding band (ESI Fig. 5b,† insert). After PEG purification the concentration of the samples were set to 10 nM with loading buffer by using a NanoPhotometer P-Class P330 (Implen, München, Germany) and the sample was incubated for at least 30 minutes. For analysis of the reaction, 50 fmol of the origami nanostructures were transferred in an agarose gel with same properties as mentioned before.

Coarse-grained simulations

The mrDNA package was used to convert caDNA no designs of the DNA origami box into a bead-based model with a resolution of approximately 5 bp per bead *via* a custom script.[37] The attractive DNA ends of the tube and lids were modeled using continuous duplex DNA in the script, precluding the possibility of unstacking. By contrast, no attractive stacking interactions were present for the repulsive ends. The ion concentration in the experiments deviates from the 25 mM $MgCl_2$ condition employed by default by the mrDNA package. Hence, the non-bonded interactions were modulated by adding a Yukawa potential with the Debye length used as a tuning parameter and subtracting a Yukawa potential with a Debye length that corresponded to the default 25 mM $MgCl_2$ condition. Comparing to TEM images of the original design, the best agreement for the box size after 2 µs simulation was obtained with a Debye length of 8.5 Å from the values: 7, 8, 8.5 and 9 Å.

Subsequently, simulations were performed of each box variant with large concentrations of different-sized cargos. The cargo molecules were represented using point particles that interact with each other and with the DNA beads through a Lennard-Jones potential with energy ε given by the geometric mean of the value for the interacting particles (0.1 kcal mol^{-1} for all cargo, 0.05 N kcal mol^{-1} for any DNA bead representing N nucleotides) and a potential minimum r_{min} determined from sum of the cargo radius (ranging from 0.4 to 2 nm) and the 1.1 nm DNA bead radius. The number of cargo particles placed in the box depended on the cargo size such that the volume was 58% full (*i.e.* 50 particles for 2 nm radius cargo). Production simulations lasted at least 200 µs. Particles were characterized as either inside or outside the box using a geometric selection, allowing the fraction of particles in each box to be plotted against the simulation time. For each cargo and each box design variant, an exponential fit yielded an estimate of the cargo escape time. The fit was applied to the last half of the data, or to the data after 50% of the cargo was depleted, whichever occurred sooner.

Author contributions

Merle Scherf: investigation, verification, visualization, writing, Florian Scheffler: investigation, Christopher Maffeo and Aleksei Aksimentiev: formal analysis, software, Ulrich Kemper and Jingjing Ye: methodology, investigation, Ralf Seidel and Uta Reibetanz: conceptualization, funding acquisition, project administration, resources, supervision, writing.

Conflicts of interest

There are no conflicts to declare.

Acknowledgements

The authors acknowledge funding from the Deutsche Forschungsgemeinschaft (DFG), in particular from grant RE 2681/5-1 to U. Reibetanz as well as grant SE 1646/8-2 and the GRK 2767 (project number 451785257) to R. Seidel. C. Maffeo and A. Aksimentiev acknowledge support from the National Science Foundation of USA (DMR-1827346) and the supercomputer time provided through the XSEDE Allocation Grant (MCA05S028) and Leadership Resource Allocation MCB20012 on Frontera of the Texas Advanced Computing Center.

References

1 N. C. Seeman and H. F. Sleiman, *Nat. Rev. Mater.*, 2018, **3**, 17068.
2 J. Kim, D. Jang, H. Park, S. Jung, D. H. Kim and W. J. Kim, *Adv. Mater.*, 2018, **30**, 1707351.
3 H. Ijäs, S. Nummelin, B. Shen, M. A. Kostiainen and V. Linko, *Int. J. Mol. Sci.*, 2018, **19**, 2114.
4 P. W. K. Rothemund, *Nature*, 2006, **440**, 297–302.
5 S. M. Douglas, H. Dietz, T. Liedl, B. Högberg, F. Graf and W. M. Shih, *Nature*, 2009, **459**, 414–418.
6 F. Hong, F. Zhang, Y. Liu and H. Yan, *Chem. Rev.*, 2017, **117**, 12584–12640.
7 S. M. Douglas, I. Bachelet and G. M. Church, *Science*, 2012, **335**, 831–834.
8 H. Ijäs, I. Hakaste, B. Shen, M. A. Kostiainen and V. Linko, *ACS Nano*, 2019, **13**, 5959–5967.

9 M. Endo and H. Sugiyama, *Molecules*, 2018, **23**, 1766.
10 J. Weiden and M. M. C. Bastings, *Curr. Opin. Colloid Interface Sci.*, 2021, **52**, 101411.
11 X. Lu, J. Liu, X. Wu and B. Ding, *Chem. – Asian J.*, 2019, **14**, 2193–2202.
12 D. Zhao, Y. Kong, S. Zhao and H. Xing, *Top. Curr. Chem.*, 2020, **378**, 41.
13 A. Fragasso, N. De Franceschi, P. Stömmer, E. O. van der Sluis, H. Dietz and C. Dekker, *ACS Nano*, 2021, **15**, 12768–12779.
14 M. Liu, J. Fu, X. Qi, S. Wootten, N. W. Woodbury, Y. Liu and H. Yan, *ChemBioChem*, 2016, **17**, 1097–1101.
15 S. K. Vittala and D. Han, *ACS Appl. Bio Mater.*, 2020, **3**, 2702–2722.
16 J. Ye, O. Aftenieva, T. Bayrak, A. Jain, T. A. F. König and A. R. Seidel, *Adv. Mater.*, 2021, **33**, 2100381.
17 L. Dai, P. Liu, X. Hu, X. Zhao, G. Shao and Y. Tian, *Analyst*, 2021, **146**, 1807–1819.
18 Z. Zhao, Y. Han and Y. Liu, *Opt. Mater. Express*, 2022, **12**, 284–3037.
19 Q. Mei, X. Wei, F. Su, Y. Liu, C. Youngbull, R. Johnson, S. Lindsay, H. Yan and D. Meldrum, *Nano Lett.*, 2011, **11**, 1477–1482.
20 N. Ponnuswamy, M. M. C. Bastings, B. Nathwani, J. H. Rye, L. Y. T. Chou, M. Vinther, W. A. Li, F. M. Anastassacos, D. J. Mooney and W. M. Shih, *Nat. Commun.*, 2017, **8**, 15654.
21 N. P. Agarwal, M. Matthies, F. N. Gür, K. Osada and T. L. Schmidt, *Angew. Chem., Int. Ed.*, 2017, **56**, 5460–5464.
22 F. M. Anastassacos, Z. Zhao, Y. Zeng and W. M. Shih, *J. Am. Chem. Soc.*, 2020, **142**, 3311–3315.
23 F. Scheffler, M. Brueckner, J. Ye, R. Seidel and U. Reibetanz, *Adv. Funct. Mater.*, 2019, **29**, 1808116.
24 H. Ijäs, B. Shen, A. Heuer-Jungemann, A. Keller, M. A. Kostiainen, T. Liedl, J. A. Ihalainen and V. Linko, *Nucleic Acids Res.*, 2021, **49**, 3048–3062.
25 I. Seitz, H. Ijäs, V. Linko and M. A. Kostiainen, *ACS Appl. Mater. Interfaces*, 2022, **14**, 38515–38524.
26 P. D. Halley, C. R. Lucas, E. M. McWilliams, M. J. Webber, R. A. Patton, C. Kural, D. M. Lucas, J. C. Byrd and C. E. Castro, *Small*, 2016, **12**, 308–320.
27 D. H. Schaffert, A. H. Okholm, R. S. Sørensen, J. S. Nielsen, T. Tørring, C. B. Rosen, A. L. B. Kodal, M. R. Mortensen, K. V. Gothelf and J. Kjems, *Small*, 2016, **12**, 2634–2640.
28 Z. Ge, L. Guo, G. Wu, J. Li, Y. Sun, Y. Hou, J. Shi, S. Song, L. Wang, C. Fan, H. Lu and Q. Li, *Small*, 2020, **16**, 1904857.
29 Z. Zhao, J. Fu, S. Dhakal, A. Johnson-Buck, M. Liu, T. Zhang, N. W. Woodbury, Y. Liu, N. G. Walter and H. Yan, *Nat. Commun.*, 2016, **7**, 10619.
30 E. S. Andersen, M. Dong, M. M. Nielsen, K. Jahn, R. Subramani, W. Mamdouh, M. M. Golas, B. Sander, H. Stark, C. L. P. Oliveira, J. S. Pedersen, V. Birkedal, F. Besenbacher, K. V. Gothelf and J. Kjems, *Nature*, 2009, **459**, 73–76.
31 G. Grossi, M. D. E. Jepsen, J. Kjems and E. S. Andersen, *Nat. Commun.*, 2017, **8**, 2.
32 A. Mukhortava and M. Schlierf, *Bioconjugate Chem.*, 2016, **27**, 1559–1563.
33 D. Y. Zhang and G. Seelig, *Nat. Chem.*, 2011, **3**, 103–113.
34 P. Irmisch, T. E. Ouldridge and R. Seidel, *J. Am. Chem. Soc.*, 2020, **142**, 11451–11463.
35 J. Ye, S. Helmi, J. Teske and R. Seidel, *Nano Lett.*, 2019, **19**, 2707–2714.
36 S. Fischer, C. Hartl, K. Frank, J. O. Rädler, T. Liedl and B. Nickel, *Nano Lett.*, 2016, **16**, 4282–4287.
37 C. Maffeo and A. Aksimentiev, *Nucleic Acids Res.*, 2020, **48**, 5135–5146.
38 D. Winogradoff, H.-Y. Chou, C. Maffeo and A. Aksimentiev, *Nat. Commun.*, 2022, **13**, 5138.
39 J. Ye, R. Weichelt, U. Kemper, V. Gupta, T. A. F. König, A. Eychmüller and R. Seidel, *Small*, 2020, **16**, 2003662.
40 L. Qin, H. Zhang, Y. Zhou, C. S. Umeshappa and H. Gao, *Small*, 2021, **17**, 2006000.
41 Y. Zhang, D. A. Davis, K. AboulFotouh, J. Wang, D. Williams, A. Bhambhani, M. Zakrewsky, M. Maniruzzaman, Z. Cui and R. O. Williams, III, *Adv. Drug Delivery Rev.*, 2021, **172**, 183–210.
42 Y. S. Loo, R. J. C. Bose, J. R. McCarthy, I. D. M. Azmi and T. Madheswaran, *Drug Discovery Today*, 2021, **26**, 902–915.
43 P. Jana, M. Shyam, S. Singh, V. Jayaprakash and A. Dev, *Eur. Polym. J.*, 2021, **142**, 110155.
44 S. M. Douglas, A. H. Marblestone, S. Teerapittayanon, A. Vazquez, G. M. Church and W. M. Shih, *Nucleic Acids Res.*, 2009, **37**, 5001–5006.
45 E. Stahl, T. G. Martin, F. Praetorius and H. Dietz, *Angew. Chem., Int. Ed.*, 2014, **53**, 12735–12740.